Electronic charges and electric potential at LaAlO_{3}/SrTiO_{3} interfaces studied by core-level photoemission spectroscopy

M. Takizawa, S. Tsuda, T. Susaki, H. Y. Hwang, and A. Fujimori

Electronic charges and electric potential at $LaAlO_3$/$SrTiO_3$ interfaces studied by core-level photoemission spectroscopy

M. Takizawa,[1] S. Tsuda,[2] T. Susaki,[2] H. Y. Hwang,[2, 3, 4] and A. Fujimori[1]

[1]*Department of Physics, University of Tokyo, 3-7-1 Hongo, Bunkyo-ku, Tokyo, 113-0033, Japan*
[2]*Department of Advanced Materials Science, University of Tokyo,*
5-1-5 Kashiwanoha, Kashiwashi, Chiba, 277-8651, Japan
[3]*Japan Science and Technology Agency, Kawaguchi, 332-0012, Japan*
[4]*Department of Applied Physics and Stanford Institute for Materials and Energy Science,*
Stanford University, Stanford, California 94305, USA
(Dated: December 1, 2011)

We studied $LaAlO_3$/$SrTiO_3$ interfaces for varying $LaAlO_3$ thickness by core-level photoemission spectroscopy. In Ti $2p$ spectra for conducting "n-type" interfaces, Ti^{3+} signals appeared, which were absent for insulating "p-type" interfaces. The intensity of the Ti^{3+} signals was significantly higher than that expected for the transport carrier densities, indicating that part of the carriers at the interfaces are localized. The Ti^{3+} signals increased with $LaAlO_3$ thickness, but started well below the critical thickness of 4 unit cells for metallic transport. Core-level shifts with $LaAlO_3$ thickness were much smaller than predicted by the polar catastrophe model. We attribute these observations to surface defects/adsorbates providing charges to the interface even below the critical thickness.

PACS numbers: 73.20.-r, 73.40.-c, 73.90.+f, 79.60.Jv

Recently, heterostructures consisting of two different metal oxides have attracted considerable interest because of their fundamental interest as well as their possible device applications. At the interfaces between two band insulators, $LaAlO_3$ and $SrTiO_3$, metallic conduction with high carrier mobility[1] and even superconductivity[2] have been observed. The transport at the $LaAlO_3$/$SrTiO_3$ interfaces shows a remarkable termination-layer dependence[1]. That is, the $(LaO)^+$/$(TiO_2)^0$ interfaces exhibit metallic conductivity while the $(AlO_2)^-$/$(SrO)^0$ interfaces remain insulating. Moreover, the metallic transport at the $LaAlO_3$/$SrTiO_3$ interfaces occurs only beyond a critical $LaAlO_3$ layer thickness of 4-6 unit cells (uc), i.e., 1.6-2.3 nm[3,4].

In order to interpret such properties of the interfaces, an electronic reconstruction which avoids a "polar catastrophe" has been proposed[5–8]. Because the (001) planes of $LaAlO_3$ are polar, that is, positively charged $(LaO)^+$ and negatively charged $(AlO_2)^-$ are alternatingly stacked, the electrostatic potential difference between both surfaces of the $LaAlO_3$(001) thin film should increase proportionally to the thickness of the $LaAlO_3$ layer. To avoid such an energetically unfavorable divergence of electrostatic potential, some charge redistribution or electronic reconstruction should take place. For the $(LaO)^+$/$(TiO_2)^0$ interfaces ("n-type" interfaces), the polar catastrophe can be avoided if half an electron is added to the interfacial region, resulting in the conversion of the valence of interface Ti atoms from the original Ti^{4+} to Ti^{4+}-Ti^{3+} mixed valence. For the $(AlO_2)^-$/$(SrO)^0$ interfaces ("p-type" interfaces), the divergence can be avoided if half an electron is removed from the interface through hole doping into the O $2p$ band or through the formation of oxygen vacancies. On the other hand, some studies[9–11] have suggested that the interfacial conductivity originated from the formation of oxygen va-

cancies in the entire region of the $SrTiO_3$[12]. A cross-sectional conducting-tip atomic force microscope study of $LaAlO_3$/$SrTiO_3$ interfaces[13] has revealed that the high-mobility electron gas is confined within a few nanometers when annealed in oxygen atmosphere. A recent study has shown that not only the carrier density but also the carrier mobility is a strong function of the $LaAlO_3$ layer thickness[14]. Indeed, the generally low carrier concentration deduced from transport measurements compared to that necessary to avoid the polar catastrophe, as well as recent experimental[15] and theoretical[16,17] studies, have pointed to major effects of carrier localization at the interfaces even above the critical $LaAlO_3$-layer thickness. Thus the origin of the metallic interfacial conductivity still remains highly controversial and is becoming even more non-trivial.

Photoemission spectroscopy (PES), which has been extensively used to study surface and bulk properties of solids, has been found to be a powerful technique to investigate oxide interfaces as well[12,18–22]. A hard x-ray PES study of the Ti core level[20] has shown that a few percent of Ti^{3+} exist within a few nanometers of the n-type $LaAlO_3$/$SrTiO_3$ interface, indicating the electronic reconstruction. However, according to an x-ray photoemission (XPS) study of both n-type and p-type $LaAlO_3$/$SrTiO_3$ interfaces[23], the core-level shifts were much smaller than and opposite to those predicted by the polar catastrophe model. Soft x-ray PES studies of the valence band and core levels have also been performed on the same systems by Yoshimatsu *et al.*[21]. They deduced the band bending on the $SrTiO_3$ side of the interface from the Ti $2p$ core-level shift with varying $LaAlO_3$ thickness, and attributed the metallic conductivity to electrons trapped by the triangular potential at the interface, although they could not detect electrons which should be doped into the Ti $3d$ band at
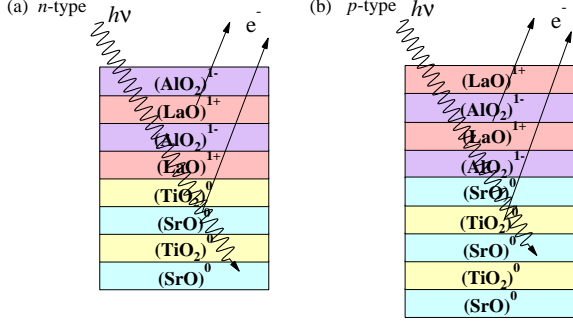
FIG. 1: (Color online) Schematic view of LaAlO$_3$ thin films grown on SrTiO$_3$ (001) substrates and their photoemission measurement geometry. Panels (a) and (b) represent the two types of samples assuming bulk-like charge assignments. (a) LaAlO$_3$ is deposited on a TiO$_2$-terminated SrTiO$_3$ substrate forming the "n-type" interface. (b) LaAlO$_3$ is deposited on a SrO-terminated SrTiO$_3$ substrate forming the "p-type" interface.

FIG. 2: (Color online) Sheet conductivity of the n-type LaAlO$_3$/SrTiO$_3$ (001) samples with varying LaAlO$_3$-layer thickness.

the LaAlO$_3$/SrTiO$_3$ interface. In a subsequent soft x-ray PES study by Drera et $al.$[22], however, the doped Ti 3d electrons were observed around the Fermi level. In the present work, in order to resolve the origins of the apparently conflicting results and clarify the electronic structure of the LaAlO$_3$/SrTiO$_3$ interface, we have performed core-level XPS measurements with varying LaAlO$_3$ thickness both for n-type and p-type interfaces. The results showed a systematic increase of the Ti^{3+} component in the Ti 2p core-level spectra with LaAlO$_3$-layer thickness only for n-type interfaces, consistent with the electronic reconstruction, whereas there was no abrupt increase at the critical LaAlO$_3$-layer thickness of $\sim$ 4 uc, and no clear core-level shifts for p-type interfaces. In order to interpret the experimental results, we suggest that the influence of charged surface defects has to be incorporated.

LaAlO$_3$ thin films with varying thickness from 1 to 6 uc were grown on the atomically flat, TiO$_2$-terminated (001) surfaces of SrTiO$_3$ substrates using pulsed laser deposition (PLD). As schematically shown in Fig. 1(a), the n-type interface is formed when the LaAlO$_3$ thin film is deposited onto this TiO$_2$-terminated surface of the SrTiO$_3$ substrate. The p-type interface is formed when the LaAlO$_3$ thin film is deposited onto the SrO-terminated surface of the SrTiO$_3$ substrate [Fig. 1(b)]. Here, the TiO$_2$-terminated surface of the SrTiO$_3$ (001) substrates could be converted to a SrO-terminated surface by depositing one unit cell of SrO. The heterostructures were grown at 600 °C under an oxygen partial pressure of 1×10^{-5} Torr. Under this condition, the carriers are considered to be confined in the interfacial region of a few nm thickness[13]. As shown in the Fig. 2, the thickness dependence of the electrical conductivity of these samples is in good agreement with that reported in the
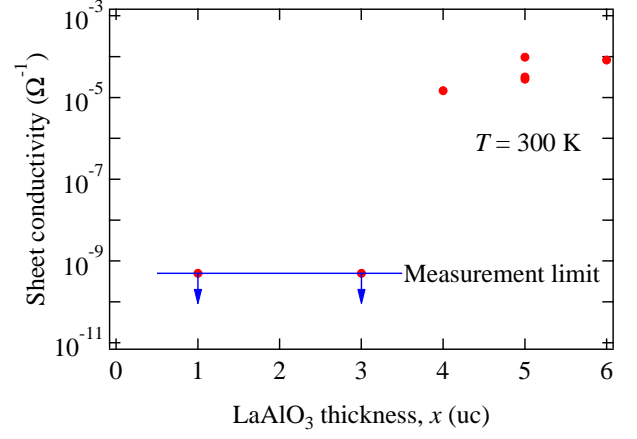
literature[4]. XPS measurements were performed using a Scienta SES-100 electron-energy analyzer and a Mg Kα ($h\nu$ = 1253.6 eV) source. Samples were transferred from the PLD chamber to the spectrometer chamber ex $situ$ and no surface treatment was performed prior to the PES measurements. All the measurements were carried out at room temperature with the total energy resolution of about 800 meV.

Figure 3 shows the La, Al, and Sr core-level spectra of the LaAlO$_3$ thin films grown on the termination-layer-controlled SrTiO$_3$ substrates as described above. Because of unavoidable charging effects of the entire sample and resultant uncertainties in the absolute binding energies, the spectra have been aligned to the peak position of the Sr 3d core level. All the spectra have been normalized to the intensity of the Sr 3d core level. With increasing LaAlO$_3$ thickness, the intensity of the La and Al core level systematically increases.

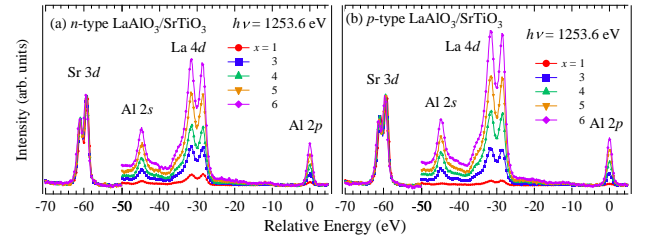FIG. 3: (Color online) La, Al, and Sr core-level spectra of the LaAlO$_3$(x uc)/SrTiO$_3$ (001) samples with varying LaAlO$_3$-layer thickness x. (a) LaAlO$_3$ layer grown on the TiO$_2$-terminated SrTiO$_3$ substrates forming an n-type interface. (b) LaAlO$_3$ layer grown on the SrO-terminated SrTiO$_3$ substrates forming a p-type interface. All the spectra have been normalized to the area of the Sr 3d core-level spectrum and the Sr 3d core-level peak positions have been aligned.
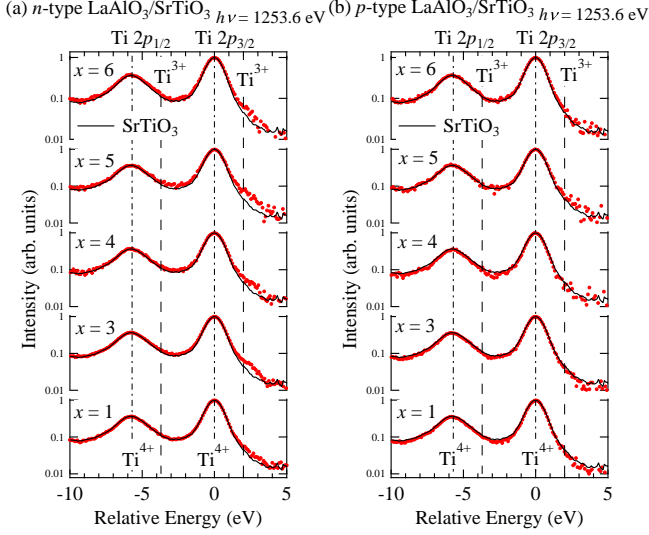
FIG. 4: (Color online) Ti $2p$ core-level spectra of LaAlO$_3$(x uc)/SrTiO$_3$ (001) samples with varying LaAlO$_3$-layer thickness x plotted on the logarithmic scale. The solid curves show the spectrum of SrTiO$_3$. (a) LaAlO$_3$ layers grown on the TiO$_2$-terminated SrTiO$_3$ substrates forming n-type interfaces. (b) LaAlO$_3$ layers grown on the SrO-terminated SrTiO$_3$ substrates forming p-type interfaces.

FIG. 5: (Color online) Ti^{3+} intensity ratio of the Ti $2p$ core-level spectra as a function of x. The dashed curve is a guide to the eye. Inset: Ti $2p$ spectrum of the $x = 6$ sample and its fitted curves. Two solid curves show those with different parameters yielding the range of error bars. The dashed curve shows the Ti^{4+} spectrum.

Figure 4 shows the Ti $2p$ core-level spectra of the same samples. The spectra have been aligned to the Ti $2p_{3/2}$ peak position and normalized to its peak height. For the LaAlO$_3$ thin films grown on TiO$_2$-terminated SrTiO$_3$ substrates forming n-type interfaces [Fig. 4(a)], one can see an additional feature which can be assigned to Ti^{3+}[24] on the lower binding-energy side of the Ti $2p_{3/2}$ peak and grows with the LaAlO$_3$-layer thickness. In order to estimate the amount of the Ti^{3+} signal, we have evaluated the area of the Ti^{3+} components by a standard line-shape fitting. As for the p-type interfaces, as shown in Fig 4(b), we find no or very little indication of Ti^{3+} signals within our experimental errors. Figure 5 shows the resulting Ti^{3+} intensity as a function of the LaAlO$_3$-layer thickness. The inset shows how we have estimated the Ti^{3+} intensity with error bars, i.e., two model curves of Ti core levels are overlaid to estimate the upper and lower limits of the Ti^{3+} intensity. Already for thickness as small as 1 uc, a weak Ti^{3+} component (~ 1 % of the Ti^{4+} peak) appeared and grew to ~ 3 % for thicknesses greater than 3 uc. Combining this Ti^{3+}/Ti^{4+} intensity ratio and the mean-free path of photoelectrons of ~ 2 nm (~ 5 uc), the total amount of Ti^{3+} per 2D unit cells is estimated to be at least 0.10 - 0.15[25], and the 2D carrier density is estimated to be at least $\sim 10^{14}$ cm^{-2}, significantly larger than $\sim 2 \times 10^{13}$ cm^{-24} estimated from the transport measurements. This indicates that a considerable portion of electrons at the n-type interfaces are localized.

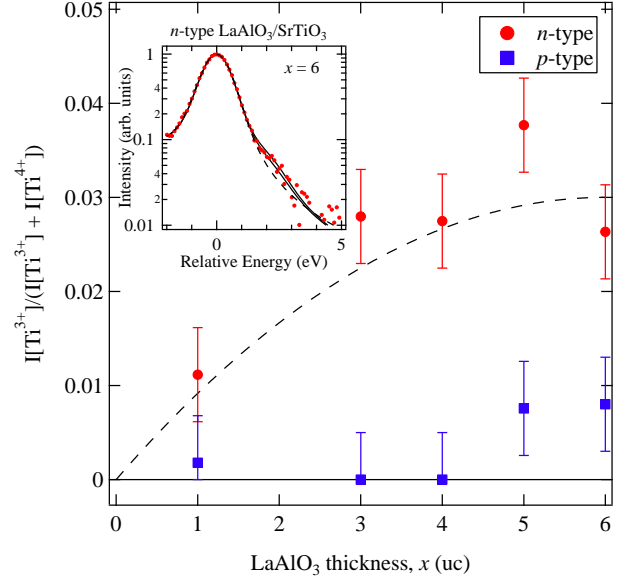Another point to note is that, while the transport data show an abrupt increase of conductivity above the critical LaAlO$_3$-layer thickness of 4 uc, the Ti^{3+} intensity started to increase gradually well below 4 uc. This suggests that the electronic reconstruction or charge transfer to the interfacial region occurred already below the critical thickness as reported in a previous work[26]. A similar behavior was also observed in polar multilayers LaAlO$_3$/LaVO$_3$/LaAlO$_3$[27,28], suggesting that the transport properties of interfaces, which show an abrupt change at 4 uc, are not solely determined by the carrier number but also by the carrier mobility[14], perhaps involving a percolation threshold. As the origin of the gradual electronic reconstruction, we consider surface defects and/or adsorbed molecules on the LaAlO$_3$ surface, such as oxygen vacancies which generate and donate electrons to the n-type interface. A similar mechanism has been discussed by Cen et $al.$ to explain the creation of metallic regions using a conducting AFM tip[29]. This mechanism has been taken into account in the theoretical description of the LaAlO$_3$/SrTiO$_3$ interface by Bristowe et $al.$[30]. According to their calculation, the Ti^{3+} component gradually appears below the critical thickness and reproduces our experimental observation of Ti^{3+} below 4 uc (Fig. 5). In fact, a recent study has shown that adsorption of polar solvents on the surface of LaAlO$_3$/SrTiO$_3$ samples induces charge carrier at the interface, indicating remote charge transfer from the surface to the interface[31]. The difference between the amount of Ti^{3+} determined by photoemission and the carrier density determined by the transport measurements below 4 uc indicates that all the
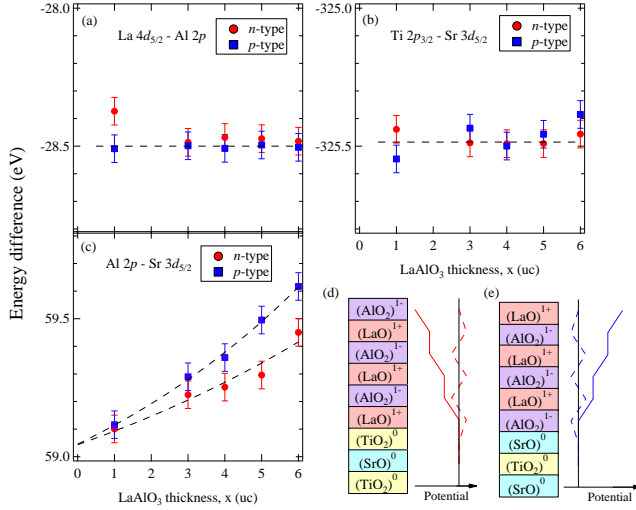
FIG. 6: (Color online) Shifts of core levels for $LaAlO_3(x$ uc) thin films grown on the $SrTiO_3$ substrates. (a) Relative shifts within the $LaAlO_3$ layers. (b) Relative shifts within the $SrTiO_3$ substrates. (c) Relative shifts between the $LaAlO_3$ and $SrTiO_3$ layers. (d),(e) Schematic diagram of the Madelung potential in the $LaAlO_3/SrTiO_3$ samples with the n-type and p-type interfaces. The dashed and solid curves represent the electrostatic potential with and without electronic reconstruction, respectively.

carriers in the Ti $3d$ band are localized below 4 uc[31].

We have also studied the core-level shifts as functions of the $LaAlO_3$-layer thickness as shown in Fig. 6. Figure 6(a) and (b) indicates that, with increasing $LaAlO_3$ thickness, all the core levels of $LaAlO_3$ are shifted by the same amount [Fig. 6(a)] and those of $SrTiO_3$ are also shifted by the same amount [Fig. 6(b)] (including charging effects), while the core levels of $LaAlO_3$ and those in $SrTiO_3$ are shifted to a different degree [Fig. 6(c)]. Considering the fact that the intensity of photoemission signals decreases exponentially with depth, the shifts of the La and Al core levels represent the electrostatic potential at the surface and those of Sr and Ti core levels represent the electrostatic potential at the interface. According to the polar catastrophe model, the shift should be as large as ~ 1 eV/uc until the critical thickness of 4 uc is reached, where the top of the O $2p$ band at the $LaAlO_3$ surface is raised above the bottom of the Ti $3d$ band of $SrTiO_3$. Figure 6(c) indicates that the experimental core-level shifts of the $LaAlO_3$ layer relative to those of the $SrTiO_3$ were less than ~ 0.1 eV/uc. Furthermore, the relative shifts were in the same direction for the n-type and p-type interfaces, in contrast to the expecta-

tions of the polar catastrophe model shown in Fig. 6(d) and (e). In Ref.[23], the shifts were also small but the relative shifts between the n-type and p-type interfaces were opposite to the present result. The existence of charged defects at the surface and resulting charge transfer from the surface to the interface explain the reduction of the core-level shifts from ~ 1 eV/uc to ~ 0.1 eV/uc, but the remaining small shifts may depend on the subtle charge distribution and may vary between the samples prepared by the MBE method[23] and the present PLD method. The remaining shifts are of the same order of magnitude as the potential shift (~ 0.3 eV/uc) calculated from the bult-in potential of the $LaAlO_3/SrTiO_3$ interface[32]. The difference likely arises from the different $LaAlO_3$ surface conditions (metal coated versus bare *ex situ* surface)[31]. The effect of surface charges on the interfacial charges suggested here needs to be confirmed by future studies with the amount of surface charges controlled.

In conclusion, we have performed a core-level photoemission spectroscopy study of $LaAlO_3/SrTiO_3$ interfaces as a function of $LaAlO_3$-layer thickness. Only for $LaAlO_3$ grown on TiO_2-terminated $SrTiO_3$ substrates (n-type interface), the Ti $2p$ core-level spectra showed a Ti^{3+} component in addition to Ti^{4+}. The amount of the Ti^{3+} component was significantly larger than the carrier densities estimated from transport measurements, indicating that part of the carriers at the interfaces are localized. The gradual rather than abrupt appearance of the Ti^{3+} component with the growth of the $LaAlO_3$ layer as well as the absence of the large core-level shifts expected from the polar catastrophe model suggests that the evolution of charged surface defects or adsorbates needs to be involved beyond the simplest polar catastrophe model[30]. These findings suggest a strong sensitivity of polar layers[28] to the electrostatic boundary conditions at the surface and interface, particularly in the perovskite heterostructures recently developed via atomic scale growth techniques. Specifically, the electronic structure near the surface is quite different when comparing an *in situ* grown surface, *ex situ*, or with further surface coverage. This aspect should be considered in the comparison of various spectroscopic studies of the surface, and present a general approach to manipulating the interface electronic structure.

[1] A. Ohtomo and H. Y. Hwang, Nature **427**, 423 (2004).
[2] N. Reyren, S. Thiel, A. D. Caviglia, L. F. Kourkoutis, G. Hammerl, C. Richter, C. W. Schneider, T. Kopp, A.-S. Rüetschi, D. Jaccard, M. Gabay, D. A. Muller, J.-M.

Triscone, and J. Mannhart, Science **317**, 1196 (2007).

3 M. Huijben, G. Rijnders, D. A. Muller, S. Bals, S. V. Aert, J. Verbeeck, G. V. Tendeloo, A. Brinkman, and H. Hilgenkamp, Nature Mater. **5**, 556 (2006).

4 S. Thiel, G. Hammeri, A. Schmehl, C. W. Schneider, and J. Mannhart, Science **313**, 1942 (2006).

5 C. Noguera, J. Phys.: Condens. Mat. **12**, R367 (2000).

6 R. Hesper, L. H. Tjeng, A. Heeres, and G. A. Sawatzky, Phys. Rev. B **62**, 16046 (2000).

7 N. Nakagawa, H. Y. Hwang, and D. A. Muller, Nature Mater. **5**, 204 (2006).

8 W.-C. Lee and A. H. MacDonald, Phys. Rev. B **76**, 075339 (2007).

9 A. Kalabukhov, R. Gunnarsson, J. Börjesson, E. Olsson, T. Claeson, and D. Winkler, Phys. Rev. B **75**, 121404(R) (2007).

10 W. Siemons, G. Koster, H. Yamamoto, W. A. Harrison, G. Lucovsky, T. H. Geballe, D. H. A. Blank, and M. R. Beasley, Phys. Rev. Lett. **98**, 196802 (2007).

11 G. Herranz, M. Basletić, M. Bibes, C. Carrétéro, E. Tafra, E. Jacquet, K. Bouzehouane, C. Deranlot, A. Hamzić, J.-M. Broto, A. Barthélémy, and A. Fert, Phys. Rev. Lett. **98**, 216803 (2007).

12 W. Siemons, G. Koster, H. Yamamoto, T. H. Geballe, D. H. A. Blank, and M. R. Beasley, Phys. Rev. B **76**, 155111 (2007).

13 M. Basletic, J.-L. Maurice, C. Carrétéro, G. Herranz, O. Copie, M. Bibes, E. Jacquet, K. Bouzehouane, S. Fusil, and A. Barthélémy, Nature Mater. **7**, 621 (2008).

14 C. Bell, S. Harashima, Y. Hikita, and H. Y. Hwang, Appl. Phys. Lett. **94**, 222111 (2009).

15 D. Dikin, M. Mehta, C. Bark, C. Folkman, C. Eom, and V. Chandrasekhar, arXiv 1103.4006 (2011).

16 R. Pentcheva and W. E. Pickett, Phys. Rev. B **74**, 035112 (2006).

17 Z. S. Popovic, S. Satpathy, and R. M. Martin, Phys. Rev. Lett. **101**, 256801 (2008).

18 M. Takizawa, H. Wadati, K. Tanaka, M. Hashimoto, T. Yoshida, A. Fujimori, A. Chikamatsu, H. Kumigashira, M. Oshima, K. Shibuya, T. Mihara, T. Ohnishi, M. Lippmaa, M. Kawasaki, H. Koinuma, S. Okamoto, and A. J. Millis, Phys. Rev. Lett. **97**, 057601 (2006).

19 H. Wadati, Y. Hotta, A. Fujimori, T. Susaki, H. Y. Hwang, Y. Takata, K. Horiba, M. Matsunami, S. Shin, M. Yabashi, K. Tamasaku, Y. Nishino, and T. Ishikawa, Phys. Rev. B **77**, 045122 (2008).

20 M. Sing, G. Berner, K. Goß, A. Müller, A. Ruff, A. Wetscherek, S. Thiel, J. Mannhart, S. A. Pauli, C. W. Schneider, P. R. Willmott, M. Gorgoi, F. Schäfers, and R. Claessen, Phys. Rev. Lett. **102**, 176805 (2009).

21 K. Yoshimatsu, R. Yasuhara, H. Kumigashira, and M. Oshima, Phys. Rev. Lett. **101**, 026802 (2008).

22 G. Drera, F. Banfi, F. F. Canova, P. Borghetti, L. Sangaletti, F. Bondino, E. Magnano, J. Huijben, G. Rijnders, D. H. A. Blank, H. Hilgenkamp, and A. Brinkman, Appl. Phys. Lett. **98**, 052907 (2011).

23 Y. Segal, J. H. Ngai, J. W. Reiner, F. J. Walker, and C. H. Ahn, Phys. Rev. B **80**, 241107(R) (2009).

24 K. Morikawa, T. Mizokawa, A. Fujimori, Y. Taguchi, and Y. Tokura, Phys. Rev. B **54**, 8446 (1996).

25 Note that the estimated value of 0.10 - 0.15 Ti^{3+} per 2D uc is a lower bound because Ti^{3+} may exist beyond the photoelectron mean-free path.

26 N. Ogawa, K. Miyano, M. Hosoda, T. Higuchi, C. Bell, Y. Hikita, and H. Y. Hwang, Phys. Rev. B **80**, 081106(R) (2009).

27 T. Higuchi, Y. Hotta, T. Susaki, A. Fujimori, and H. Y. Hwang, Phys. Rev. B **79**, 075415 (2009).

28 M. Takizawa, Y. Hotta, T. Susaki, Y. Ishida, H. Wadati, Y. Takata, K. Horiba, M. Matsunami, S. Shin, M. Yabashi, K. Tamasaku, Y. Nishino, T. Ishikawa, A. Fujimori, and H. Y. Hwang, Phys. Rev. Lett. **102**, 236401 (2009).

29 C. Cen, S. Thiel, G. Hammerl, C. W. Schneider, K. E. Andersen, C. S. Hellberg, J. Mannhart, and J. Levy, Nature Mater. **7**, 298 (2008).

30 N. C. Bristowe, P. B. Littlewood, and E. Artacho, Phys. Rev. B **83**, 205405 (2011).

31 Y. Xie, Y. Hikita, C. Bell, and H. Y. Hwang, Nature Commun. **2**, 494 (2011).

32 G. Singh-Bhalla, C. Bell, J. Ravichandran, W. Siemons, Y. Hikita, S. Salahuddin, A. F. Herbard, H. Y. Hwang, and R. Ramesh, Nature Phys. **7**, 80 (2011).